PROTEINS
STRUCTURE ■ FUNCTION ■ BIOINFORMATICS

SHORT COMMUNICATION

Lipid nanotechnologies for structural studies of membrane-associated proteins

Svetla Stoilova-McPhie,[1,2]* Kirill Grushin,[1] Daniela Dalm,[1] and Jaimy Miller[1]

[1] Department of Neuroscience and Cell Biology, The University of Texas Medical Branch, 301 University Blvd, Galveston, Texas 77555

[2] Sealy Center for Structural Biology and Molecular Biophysics, The University of Texas Medical Branch, 301 University Blvd, Galveston, Texas 77555

ABSTRACT

We present a methodology of lipid nanotubes (LNT) and nanodisks technologies optimized in our laboratory for structural studies of membrane-associated proteins at close to physiological conditions. The application of these lipid nanotechnologies for structure determination by cryo-electron microscopy (cryo-EM) is fundamental for understanding and modulating their function. The LNTs in our studies are single bilayer galactosylceramide based nanotubes of ~20 nm inner diameter and a few microns in length, that self-assemble in aqueous solutions. The lipid nanodisks (NDs) are self-assembled discoid lipid bilayers of ~10 nm diameter, which are stabilized in aqueous solutions by a belt of amphipathic helical scaffold proteins. By combining LNT and ND technologies, we can examine structurally how the membrane curvature and lipid composition modulates the function of the membrane-associated proteins. As proof of principle, we have engineered these lipid nanotechnologies to mimic the activated platelet's phosphtaidylserine rich membrane and have successfully assembled functional membrane-bound coagulation factor VIII *in vitro* for structure determination by cryo-EM. The macromolecular organization of the proteins bound to ND and LNT are further defined by fitting the known atomic structures within the calculated three-dimensional maps. The combination of LNT and ND technologies offers a means to control the design and assembly of a wide range of functional membrane-associated proteins and complexes for structural studies by cryo-EM. The presented results confirm the suitability of the developed methodology for studying the functional structure of membrane-associated proteins, such as the coagulation factors, at a close to physiological environment.

Proteins 2014; 00:000–000.
© 2014 Wiley Periodicals, Inc.

Key words: lipid nanotubes; lipid nanodisks; membrane-associated proteins; cryoelectron microscopy; protein structure.

INTRODUCTION

Although information on the structure and oligomeric organization of proteins in solution is extensive, obtaining data on membrane-associated proteins has been challenging. This is due to the intrinsic complexity of cell membranes and the large size of membrane-bound protein assemblies, which renders them difficult to study by standard structural methods, such as X-ray crystallography, and nuclear magnetic resonance (NMR).[1–3] Therefore there is a gap to fill by developing model lipid nanosystems specifically suited for structural studies of peripheral membrane proteins and complexes, which are distinct from the existing membrane mimetics optimized for structural studies of integral membrane proteins, such as liposomes, micelles, bicelles, and cubic phases.[2,4–8] The traditional structural environment for

Additional Supporting Information may be found in the online version of this article.

Grant sponsor: National Scientist Development grant from the American Heart Association; grant number: 10SDG3500034; Grant sponsor: UTMB (to SSM).

*Correspondence to: Svetla Stoilova-McPhie, Department of Neuroscience and Cell Biology, The University of Texas Medical Branch, 301 University Blvd, Galveston, TX 77555. E-mail: svmcphie@utmb.edu or www.svetla-mcphie-cryoem.com

Received 19 April 2014; Revised 4 June 2014; Accepted 8 June 2014
Published online 23 June 2014 in Wiley Online Library (wileyonlinelibrary.com).
DOI: 10.1002/prot.24631

integral membrane proteins *in vitro* requires detergents to achieve sufficient solubility of the proteins and preserve their functional structure.[9,10] In the case of peripheral membrane proteins, detergents cannot be used for structural and functional studies as they affect the lipid membrane integrity and fluidity, modifying the membrane surface and protein–lipid interaction such as to affect their structure and function.[7,9,11] The presented research focuses on optimizing lipid nanotubes (LNT) and nanodisks (NDs) at the same lipid compositions for structural determination of functional membrane-associated proteins by cryoelectron microscopy (cryo-EM).

Single bilayer LNT self-assemble from solubilized lipid mixtures containing 20% or more galactosylceramide (GC) in aqueous buffered solutions.[12,13] GC-LNT have a stable inner diameter of ~20 nm and can reach a few microns in length. LNT are suitable for helical organization of soluble proteins and complexes allowing near atomic structure determination by cryo-EM.[14–16] The advantage of LNT over lipid monolayers, vesicles, and ND is that they are close to *in vivo* bilayer systems by curvature and compartmentalization, can mimic native lipid composition and are more uniform in diameter than liposomes. Structural studies of helically organized proteins bound to LNT by cryo-EM are also favored as they do not require tilting of the specimen for high-resolution data acquisition as is the case for two-dimensional (2D) crystals, as all views in a helical crystal are presented in the planar images.[16–18] The challenge of this approach however, is that it requires high quality helical crystals, which can be a lengthy trial and error process.

Single bilayer ND self-assemble in aqueous solution after dialyzing out the detergent from the mixture of lipids and amphipathic helical scaffold proteins.[19] The membrane scaffolding proteins (MPS) form a belt, which stabilizes the ND bilayer. The size of the ND can vary from 8 to 16 nm in diameter, depending of the length of the MPS and the type of lipids incorporated in the bilayer. NDs are suitable for structure–functional studies of membrane and membrane-associated proteins and complexes.[20,21] NDs have been successfully used as membrane mimetics for biophysical, biochemical, and structural studies of integral membrane proteins by NMR,[20,22,23] EM, and cryo-EM combined with single particle analysis (SPA).[22,24–26] Both ND and LNT can be used to mimic native lipid composition *in vitro*. The advantages however of using ND for structural studies by cryo-EM compared to liposomes is that they are monodisperse and do not require ordered assemblies, as do the LNT. Thus, NDs are specifically suited for large macromolecular complexes, which are less amenable to helical organization than individual proteins.[21]

LNT and ND have different geometry, curvature, and lipid phase properties, which significantly impact correctly defining the structure and function of the assembled membrane-bound proteins and complexes. Thus by using both LNT and ND nanotechnologies, we can unambiguously define the functional states of membrane-associated proteins. To demonstrate the feasibility of the proposed approach, we have organized blood coagulation factor VIII (FVIII) on functionalized LNT and ND for structural studies by EM. LNTs are morphologically similar to the activated platelet pseudopodia, which is the physiological substrate for the assembly of the coagulation proteins and complexes *in vivo*.[27–29] Lipid nanodisks have been proven to be suitable for the assembly and structural studies of blood clotting factors and complexes[30–32] at closest to physiological conditions.

Coagulation FVIII is a multidomain blood plasma protein, which when activated (FVIIIa) functions as a cofactor to the serine protease factor IXa (FIXa) in the membrane-bound Tenase (FVIIIa–FIXa) complex. Binding of FVIIIa to FIXa on the activated platelet membrane increases FIXa protelytic activity and consecutive Thrombin generation more than 100,000 times, which secures effective coagulation. Defects or deficiency of FVIII are cause for Hemophilia A, which is a severe hereditary bleeding disorder.[33] FVIII binds with high affinity to negatively charged phospholipid membranes rich in phosphatidylserine (PS, Kd ~1 n*M*) and is capable of forming 2D and helical crystals on PS containing monolayers and nanotubes.[34–36] FVIII is a large 300 kDa glycoprotein of 2332 amino acid residues organized as six domains: A1–A2–B–A3–C1–C2.[37] *In vitro*, following purification from blood plasma or after expression, FVIII exists as a mixture of heterodimers of a heavy chain (HC) of the A1–A2 domains containing parts of the B domain and a light chain (LC) of the A1–C1–C2 domains. The LC and HC are noncovalently linked via divalent Ca^{2+} ion(s).[38,39] FVIII is further activated by Thrombin, resulting in the cleavage of the entire B domain and separating the A2 and A1 domains.[40] Thus, the activated FVIII (FVIIIa) is a heterotrimer composed of noncovalently linked A1, A2 domains, and the LC. The A1 and LC retain the metal ion-dependent linkage through the A1-A3 domains, whereas the association of A2 to A1 is mediated solely by hydrophobic and electrostatic interactions.[39,41–44] FVIIIa is inherently unstable with a half-life of approximately 1–2 min *in vitro*, as the A2 domain is only weakly attached to the rest of the molecule (Kd ~ 500 μ*M*) and dissociates spontaneously resulting in loss of activity.[39–41,45–48] The structure of human recombinant FVIII lacking the B domain as organized in 3D crystals in solution has been resolved at ~4 Å by X-ray crystallography.[43,45,49] The structure of plasma derived human FVIII organized in membrane-bound 2D crystals was calculated at 15 Å by electron crystallography. Further fitting of the X-ray coordinates (3CDZ)[45] in the EM map resolved the FVIII membrane-

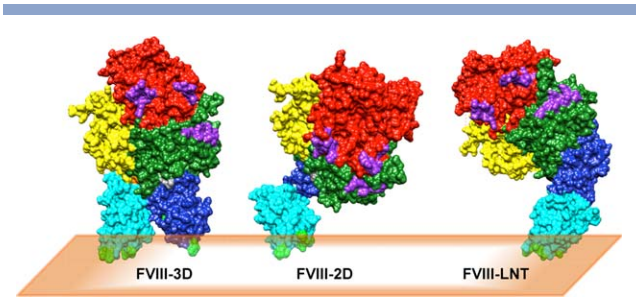

Figure 1

FVIII structures. FVIII-3D (3CDZ.PDB): structure of FVIII organized in 3D crystals in solution.[45] FVIII-2D (3J2Q.PDB): structure of FVIII organized in membrane-bound 2D crystals.[34] FVIII-LNT: structure of FVIII bound to LNT, as calculated from helically organized FVIII-LC on LNT (3J2S.PDB).[35] The five FVIII domains are indicated as: A1—yellow, A2—red, A3—green, C1—blue, and C2—cyan. The FVIII membrane-binding residues identified on the C1 and C2 domains are shown in green. The FVIII residues identified at the FVIIIa–FIXa interface are shown in purple. The lipid membrane is shown as an orange parallelepiped.

bound domain organization in the 2D crystals (3J2Q).[34,35] The structure of human recombinant FVIII-LC helically organized on LNT was calculated at 20 Å by cryo-EM. Fitting of the FVIII-LC coordinates from the X-ray structure (3CDZ) within the cryo-EM map resolved the membrane-bound FVIII-LC structure, when helically organized on LNT (3J2S).[35] Modeling of the FVIII-HC coordinates from the FVIII-2D structure (3J2Q) to the FVIII-LC-LNT structure (3J2S) was achieved by aligning the A3 domain from the FVIII-2D structure (3J2Q) to the A3 domain from the FVIII-LC-LNT structure (3J2S) resulting in the final FVIII-LNT domain organization as shown on Figure 1.[35] The orientation of the A1-A2 domains from the FVIII-HC respective to the A3 domain of the FVIII-LC in both FVIII-2D (3J2Q) and FVIII-LNT (3J2S) was preserved (Fig. 1). The membrane-bound FVIII structures, as organized in 2D[34] and helical crystals[35] show consistent differences in the domain organization compared to those of FVIII organized in 3D crystals[43,45] in solution (Fig. 1). Resolving the FVIII structure at different membrane environments is the next step toward understanding the functional implications of FVIII membrane-bound organization for blood hemostasis.

MATERIALS AND METHODS

Samples preparation

Human FVIII lacking the B domain (gift from Novo Nordisk) was purified as described.[50] Porcine FVIII (pFVIII) lacking the B domain was expressed in BHK cells and purified following the procedure described in Ref. 51. Both human and pFVIII proteins were buffer exchanged against HBS-Ca buffer (20 m*M* HEPES, 150 m*M* NaCl, 5 m*M* $CaCl_2$, pH = 7.4), concentrated to ~1 mg/mL and kept at −80°C.

LNT were prepared from GC (C24: 1 β-D-galactosyl ceramide; Avanti Polar Lipids) and PS (1,2-dioleoyl-sn-glycero-3-phospho-L-serine; Avanti Polar Lipids) mixed at 1:4 (w/w) ratio in chloroform. The chloroform was evaporated under argon and the lipid film was rehydrated in HBS buffer to a final concentration of 1 mg/mL.

NDs were prepared from the same lipids as the LNT (GC and PS) and at the same lipid composition (1:4, w/w ratio) following the procedure described in Ref. 52. The rehydrated lipid film in HBS buffer were mixed with the MSP1D1 scaffolding protein (M6574; Sigma) at 47:1 lipid to protein ratio in the presence of 15 m*M* sodium cholate. After removing the detergent by addition of Bio-Beads (SM-2; Bio-Rad) at 1 mg/mL the NDs were separated by size with a Superdex 200 HR 10/30 column. The fraction corresponding to ND with a diameter of 10 nm was used for the FVIII-ND experiments.

Cryo-EM

The FVIII-LNT samples were prepared by mixing the FVIII and LNT at 2:1 w/w ratio in HBS-Ca buffer. FVIII-LNT sample of 2.5 μL was deposited onto hydrophilic holey carbon electron microscopy grids (R2x2, Quantifoil). The excess liquid was blotted and the grids flash frozen in liquid ethane using a Vitrobot Mark III (FEI), cooled down by liquid nitrogen to obtain amorphous ice.

Cryo-EM data were collected at close to liquid nitrogen temperature (−175°C) with a JEM2100-LaB_6 (JEOL) equipped transmission electron microscope operated at 200 kV. Images were recorded with a 4096 × 4096 pixels CCD camera (US4000, Gatan Inc) at low electron dose conditions (~16 electrons/$Å^2$ s), 56,000× magnification and 2.9 Å/pixel resolution.

Electron microscopy

The FVIII-ND samples were prepared at the same FVIII to ND ratio and buffer conditions as the FVIII-LNT samples, and diluted to ~0.005 mg/mL. FVIII-ND sample of 5 μL was deposited on freshly prepared hydrophilic carbon-coated electron microscopy grids and stained with 2% uranyl acetate.

EM data from the negatively stained FVIII-ND specimen were collected at room temperature (~24°C) at the same imaging conditions and with the same equipment as the cryo-EM data.

Electron tomography

The FVIII-LNT samples were prepared as for the cryo-EM experiments. FVIII-LNT sample of 2.5 μL mixed with 6 nm colloidal gold nanoparticles was applied to the grids and negatively stained with 1% uranyl acetate. Tilt series were collected with the SerialEM software[53] at 2°

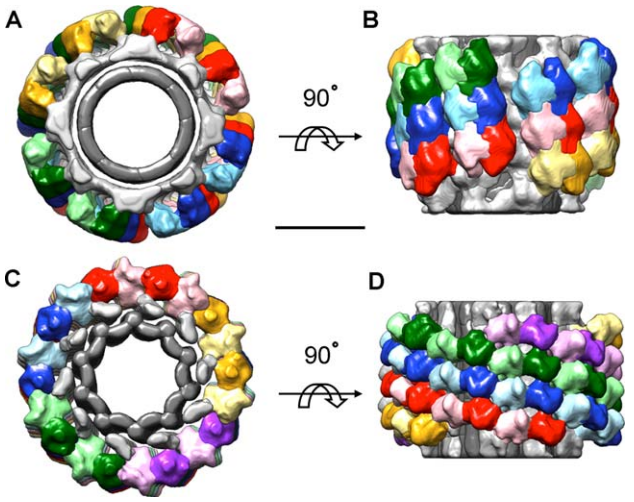

Figure 2

Helical organization of human (**A** and **B**) and porcine (**C** and **D**) FVIII bound to LNT. (A and C) Views along and (B and D) perpendicular to the helical axis. The individual FVIII-LNT helices are color-coded. The human FVIII-LNT structure is a four-start helical structure (A and B) and the porcine FVIII-LNT structure is a five-start helical structure (C and D). The inner and outer LNT monolayers are colored in dark and light gray, respectively. The density of the outer monolayer contains the FVIII membrane-associated part. The FVIII molecules within the asymmetric unit (dimer) are colored in light and dark shades. The molecules at the edge have been removed for clarity. The scale bar is 20 nm.

increments over an angular range of −60° to +60°, electron dose of 60–74 electrons/Å^2 s per tomogram and 56,000× magnification with the same electron microscope and CCD camera as the FVIII-ND samples. The tomograms were reconstructed with the IMOD software.[54]

Image analysis

2D image analysis was carried out with the EMAN2 scientific image processing suite,[55] using the e2refine2d.py iterative reference free alignment[56] algorithm based on multivariate statistical analysis implemented in EMAN2. This process was iterated several times, until homogenous data set of FVIII-LNT helical segments and FVIII-ND particles were created.[35]

Helical reconstruction was carried out from the selected human and pFVIII-LNT data sets with the iterative helical real space reconstruction (IHRSR) algorithm, as described in Refs. 35,57,58. Single particle reconstruction was carried out with the EMAN2 single particle analysis workflow.[55]

RESULTS AND DISCUSSION

FVIII organization bound to LNT

To gain more information on the conformational space of the FVIII membrane-bound molecules at close to phsyiological conditions, we have helically organized two recombinant FVIII forms, human and porcine on PS containing LNT and collected cryo-EM data as previously described.[59] pFVIII is highly homologous to the human FVIII (86% sequence identity).[60] Both proteins are clinically used for the treatment of hemophilia A, as 30% of hemophilia A patients develop inhibitory antibodies against human FVIII and pFVIII is an effective replacement.[61,62] Both recombinant FVIII forms, lack the B domain, which makes them more homogenous and stable in solution than the plasma derived FVIII and activated FVIII (FVIIIa), thus more amenable for structural studies.[60] We have optimized the helical organization of both proteins for high protein to lipid ratio (2:1, w/w) and PS to GC content (PS:GC = 4:1, w/w; Supporting Information Fig. S1). Initial 3D reconstructions for human and pFVIII helically organized on LNT were calculated from 1000 helical segments at 20 Å resolution with the IHRSR algorithm as described in Refs. 35,59. Despite the high homology in sequence and similarity in function, the human and pFVIII showed consistently different helical organizations when bound to the LNT at the same solution conditions (20 m*M* HEPES buffer, pH = 7.4, 150 m*M* NaCl and 5 m*M* $CaCl_2$; Fig. 2). The human FVIII molecules are organized as a four start and the pFVIII as a five start helical structure [Fig. 2(B,D)]. The asymmetric unit for both human and pFVIII-LNT helical assemblies is an asymmetric homodimer, consisting of two FVIII molecules (Fig. 2 and Supporting Information Fig. S2). The volume of the FVIII dimer, as shown in Figure 3(A,B), was calculated to be 989 × 10^6 Å^3 for the human and 1090 × 10^6 Å^3 for the porcine form. These volumes can accommodate well two FVIII molecules, as the volume corresponding to one FVIII molecule as calculated from the FVIII-3D structure (3CDZ) filtered at 25 Å is 495 × 10^6 Å^3. To understand the macromolecular organization of the FVIII molecules within the heterodimer, all three FVIII structures, as organized in 3D, 2D, and helical crystals shown in Figure 1, were fitted to the cryo-EM maps. This was achieved with the rigid body fitting algorithms implemented in the UCSF-Chimera molecular modeling system "fit in map" and "fit to segment" options[63–66] keeping the orientation of the FVIII molecules, such as to properly position the C2 domain residues identified to bind to the membrane (shown in green in Fig. 2). Only the fitting of the FVIII-LNT structure gave a satisfactory score for both human and pFVIII dimers (Fig. 3). The presented helical reconstructions in Figure 2 and fittings in Figure 3 confirmed the correctness of the FVIII-LNT structure previously derived from the FVIII-LC-LNT cryo-EM map.[35] The resolved differences between the human and pFVIII-LNT 3D maps showed that the proposed approach is sensitive enough to detect differences in structure due to differences in sequence between the two proteins (Figs. 2 and 3). Such differences are not detectable by biophysical and biochemical studies such as circular dichroism, sodium dodecyl sulfate-polyacrylamide gel electrophoresis, and functional tests.[60]

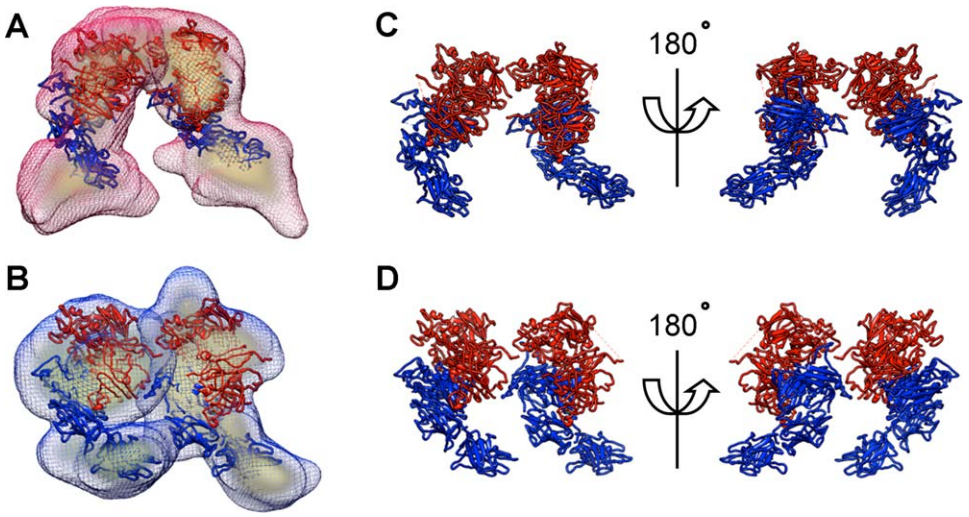

Figure 3

Fitting of the FVIII-LNT structure within the human (**A**) and porcine (**B**) FVIII-dimers cryo-EM map. The FVIII-LNT dimer (unit cell) surface is shown as a red mesh for the human (A) and blue for the porcine (B) form. The maximum density is shown as a solid yellow color. The FVIII-LNT structure (Fig. 1) is shown as ribbons. The FVIII-HC is colored in red and the FVIII-LC in blue. Organization of the FVIII molecules as fitted in the human (C) and porcine (D) FVIII-LNT dimers' CRYO-EM map.

FVIII organization bound to ND

To test how the membrane-bound FVIII molecules organize when helical order is not imposed, we optimized ND with the same lipid composition as the LNT, stabilized with MSP1D1 scaffolding proteins at a protein to lipid ratio of 1:47. The FVIII-ND complexes were obtained at the same FVIII to lipid ratio and solution conditions as the ones for the FVIII-LNT experiments. 175 micrographs of pFVIII bound to the ND were

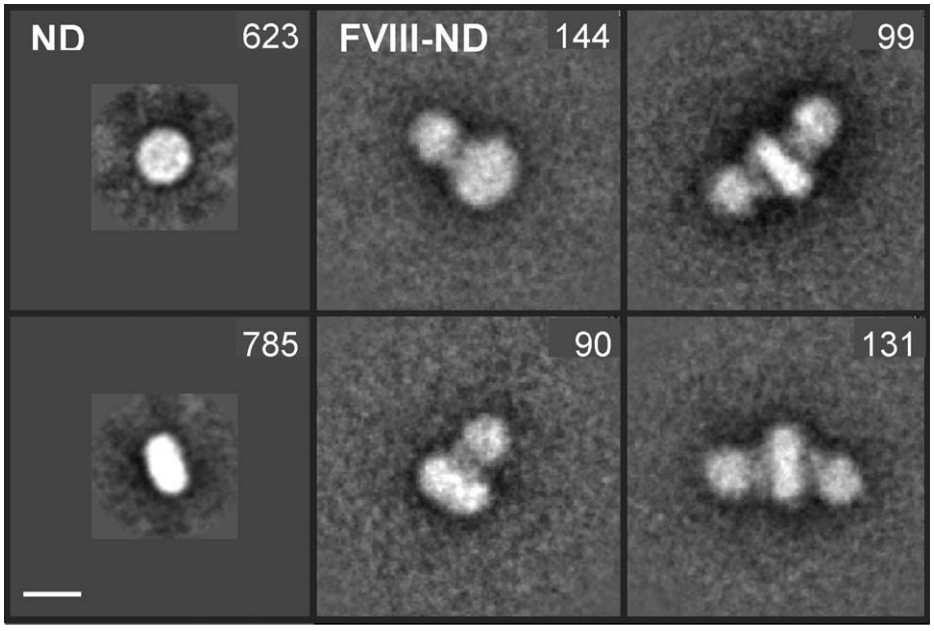

Figure 4

Representative 2D class averages from 4009 ND particles classified in 30 classes and 6387 porcine FVIII-ND particles classified in 50 classes. The ND and FVIII-ND particles are masked with 48 and 80 pixels radius masks, respectively. The number of particles in each class is indicated. The scale bar is 10 nm.

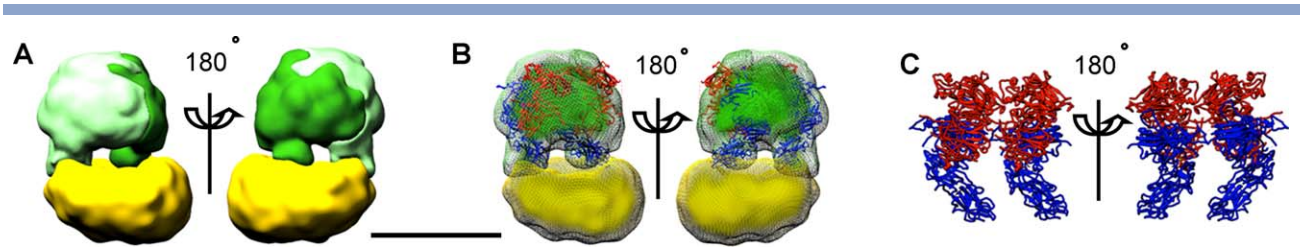

Figure 5

Structure of porcine bound to ND. (**A**) Segmentation of the FVIII-ND 3D reconstruction showing the densities corresponding to the ND in yellow and the FVIII molecules in light and dark green, respectively. (**B**) Fitting of the FVIII-LNT structure (Fig. 1) within the FVIII dimer EM map. The FVIII-LC is shown as blue ribbons and the FVIII-HC as red ribbons. (**C**) Organization of the FVIII molecules as fitted within the FVIII-ND EM map. The scale bar is 10 nm.

collected and the pFVIII-ND particles were boxed at 180 x 180 pixels (at 2.9 Å/pix) with the single particle analysis (SPA) workflow of EMAN2.[55] The initial particle set of 6387 particles was subjected to reference free 2D classification to separate the ND with FVIII bound to one side from the ND with FVIII bound to both sides of the membrane. A final data set of 2013 particles was selected for the FVIII-ND 3D reconstruction (Fig. 4 and Supporting Information Fig. S3). The FVIII-ND 3D structure was calculated at 35 Å resolution and showed two well-defined densities corresponding to the ND and the FVIII molecules. Further segmentation with the Seggers algorithms implemented in UCSF-Chimera software[66] showed a dimeric organization of the FVIII molecules bound to the ND [Fig. 5(A)]. Fitting separately the three FVIII structures shown in Figure 1 with the rigid body docking algorithms implemented in the "fit in map" option of the UCSF Chimera confirmed that the FVIII-LNT structure fitted best the FVIII-ND EM map [Fig. 5(B)]. The fact that the FVIII molecules form asymmetric homodimers when bound to both ND and LNT, and that the dimeric interface between the heavy chains of the adjacent FVIII molecules appears similar, suggests that this oligomeric organization might have functional implications and is not induced by the helical packing [Figs. 3(D) and (C)].

FVIIIa membrane-bound organization

The activated FVIII form—FVIIIa, which is the cofactor to the serine protease FIXa within the membrane-bund Tenase complex, is inherently unstable. Both FVIII and FVIIIa bind to negatively charged phospholipid membranes and to FIXa.[67] We express and purify pFVIII in our laboratory, as it has much higher yield (14×) than human FVIII, is more stable in solution and the active form (pFVIIIa) is also stable at concentration above 0.5 m*M*/mL at pH = 6.[60,67] We have successfully organized helically both pFVIII and pFVIIIa on LNT and quite similar helical organization for both pFVIII and pFVIIIa, also judged by the diffraction of the filaments (results not shown). From these observations, it looks like the differences between pFVIII and pFVIIIa membrane-bound organization will not be as pronounced as between the hFVIII and pFVIII presented in this article. We do however expect subtle difference at the level of the FVIIIa–FVIIIa and FVIIIa–FIXa interfaces.

CONCLUSIONS

The lipid nanotechnologies presented in this work are specifically suited for structural studies of large membrane-associated proteins and complexes by cryo-EM at close to physiological conditions. Our results confirm the resolving power of cryo-EM in combination with LNT and ND nanotechnologies that have different geometry and same lipid composition, for structural determination of functional membrane-associated protein complexes. Customizing the presented LNT and ND technologies to different membrane protein systems will offer a means to control the design and macromolecular organization of a wide range of functional membrane-associate proteins for structural studies by cryo-EM.

ACKNOWLEDGMENTS

The authors acknowledge the cryo-EM facility and Scientific Computing facilities at the Sealy Center for Structural Biology at the University of Texas Medical Branch. This work was also supported by a National Scientist Development grant from the American Heart Association: 10SDG3500034 and UTMB start up funds to SSM.

REFERENCES

1. Opella SJ. Structure determination of membrane proteins in their native phospholipid bilayer environment by rotationally aligned solid-state NMR spectroscopy. Acc Chem Res 2013;46:2145–2153.
2. Opella SJ. Structure determination of membrane proteins by nuclear magnetic resonance spectroscopy. Annu Rev Anal Chem (Palo Alto Calif) 2013;6:305–328.
3. Fleishman SJ, Unger VM, Ben-Tal N. Transmembrane protein structures without X-rays. Trends in biochemical sciences 2006;31:106–113.

4. Das N, Murray DT, Cross TA. Lipid bilayer preparations of membrane proteins for oriented and magic-angle spinning solid-state NMR samples. Nat Protoc 2013;8:2256–2270.
5. Liu Y, Sigworth FJ. Automatic cryo-EM particle selection for membrane proteins in spherical liposomes. J Struct Biol 2014;185:295–302.
6. ZE, O'Connell JD III, Gruswitz F, Hays FA, Harries WE, Harwood IM, Ho JD, Lee JK, Savage DF, Miercke LJ, Stroud RM. A general protocol for the crystallization of membrane proteins for X-ray structural investigation. Nat Protoc 2009;4:619–637.
7. Zhou HX, Cross TA. Influences of membrane mimetic environments on membrane protein structures. Annu Rev Biophys 2013;42: 361–392.
8. Rummel G, Hardmeyer A, Widmer C, Chiu ML, Nollert P, Locher KP, Pedruzzi II, Landau EM, Rosenbusch JP. Lipidic cubic phases: new matrices for the three-dimensional crystallization of membrane proteins. J Struct Biol 1998;121:82–91.
9. le Maire M, Champeil P, Moller JV. Interaction of membrane proteins and lipids with solubilizing detergents. Biochim Biophys Acta 2000;1508:86–111.
10. Seddon AM, Curnow P, Booth PJ. Membrane proteins, lipids and detergents: not just a soap opera. Biochim Biophys Acta 2004;1666: 105–117.
11. Almgren M. Mixed micelles and other structures in the solubilization of bilayer lipid membranes by surfactants. Biochim Biophys Acta 2000;1508:146–163.
12. Parmenter CD, Stoilova-McPhie S. Binding of recombinant human coagulation factor VIII to lipid nanotubes. FEBS Lett 2008;582: 1657–1660.
13. Parmenter CD, Cane MC, Zhang R, Stoilova-McPhie S. Cryo-electron microscopy of coagulation Factor VIII bound to lipid nanotubes. Biochem Biophys Res Commun 2008;366:288–293.
14. Wilson-Kubalek EM, Chappie JS, Arthur CP. Helical crystallization of soluble and membrane binding proteins. Methods Enzymol 2010; 481:45–62.
15. Henderson R. Realizing the potential of electron cryo-microscopy. Q Rev Biophys 2004;37:3–13.
16. Egelman EH. Reconstruction of helical filaments and tubes. Methods Enzymol 2010;482:167–183.
17. DeRosier DJ, Moore PB. Reconstruction of three-dimensional images from electron micrographs of structures with helical symmetry. J Mol Biol 1970;52:355–369.
18. Henderson R, Unwin PN. Three-dimensional model of purple membrane obtained by electron microscopy. Nature 1975;257:28–32.
19. Schuler MA, Denisov IG, Sligar SG. Nanodiscs as a new tool to examine lipid–protein interactions. Methods Mol Biol 2013;974: 415–433.
20. Bayburt TH, Sligar SG. Membrane protein assembly into nanodiscs. FEBS Lett 2010;584:1721–1727.
21. Hagn F, Etzkorn M, Raschle T, Wagner G. Optimized phospholipid bilayer nanodiscs facilitate high-resolution structure determination of membrane proteins. J Am Chem Soc 2013;135:1919–1925.
22. Kijac AZ, Li Y, Sligar SG, Rienstra CM. Magic-angle spinning solid-state NMR spectroscopy of nanodisc-embedded human CYP3A4. Biochemistry 2007;46:13696–13703.
23. Etzkorn M, Raschle T, Hagn F, Gelev V, Rice AJ, Walz T, Wagner G. Cell-free expressed bacteriorhodopsin in different soluble membrane mimetics: biophysical properties and NMR accessibility. Structure 2013;21:394–401.
24. Katayama H, Wang J, Tama F, Chollet L, Gogol EP, Collier RJ, Fisher MT. Three-dimensional structure of the anthrax toxin pore inserted into lipid nanodiscs and lipid vesicles. Proc Natl Acad Sci USA 2010;107:3453–3457.
25. Ye F, Hu G, Taylor D, Ratnikov B, Bobkov AA, McLean MA, Sligar SG, Taylor KA, Ginsberg MH. Recreation of the terminal events in physiological integrin activation. J Cell Biol 2010;188:157–173.
26. Raschle T, Hiller S, Yu TY, Rice AJ, Walz T, Wagner G. Structural and functional characterization of the integral membrane protein VDAC-1 in lipid bilayer nanodiscs. J Am Chem Soc 2009;131: 17777–17779.
27. Hensler ME, Frojmovic M, Taylor RG, Hantgan RR, Lewis JC. Platelet morphologic changes and fibrinogen receptor localization. Initial responses in ADP-activated human platelets. Am J Pathol 1992;141: 707–719.
28. Bevers EM, Comfurius P, van Rijn JL, Hemker HC, Zwaal RF. Generation of prothrombin-converting activity and the exposure of phosphatidylserine at the outer surface of platelets. Eur J Biochem 1982;122:429–436.
29. Williamson P, Bevers EM, Smeets EF, Comfurius P, Schlegel RA, Zwaal RF. Continuous analysis of the mechanism of activated transbilayer lipid movement in platelets. Biochemistry 1995;34:10448–10455.
30. Morrissey JH, Pureza V, Davis-Harrison RL, Sligar SG, Rienstra CM, Kijac AZ, Ohkubo YZ, Tajkhorshid E. Protein–membrane interactions: blood clotting on nanoscale bilayers. J Thromb Haemost 2009;7 Suppl 1:169–172.
31. Morrissey JH, Tajkhorshid E, Rienstra CM. Nanoscale studies of protein–membrane interactions in blood clotting. J Thromb Haemost 2011;9 Suppl 1:162–167.
32. Ohkubo YZ, Morrissey JH, Tajkhorshid E. Dynamical view of membrane binding and complex formation of human factor VIIa and tissue factor. J Thromb Haemost 2010;8:1044–1053.
33. Hoyer LW. Hemophilia A. N E J Med 1994;330:38–47.
34. Stoilova-McPhie S, Villoutreix BO, Mertens K, Kemball-Cook G, Holzenburg A. 3-Dimensional structure of membrane-bound coagulation factor VIII: modeling of the factor VIII heterodimer within a 3-dimensional density map derived by electron crystallography. Blood 2002;99:1215–1223.
35. Stoilova-McPhie S, Lynch GC, Ludtke S, Pettitt BM. Domain organization of membrane-bound factor VIII. Biopolymers 2013;99:448–459.
36. Stoylova SS, Lenting PJ, Kemball-Cook G, Holzenburg A. Electron crystallography of human blood coagulation factor VIII bound to phospholipid monolayers. J Biol Chem 1999;274:36573–36578.
37. Vehar GA, Keyt B, Eaton D, Rodriguez H, O'Brien DP, Rotblat F, Oppermann H, Keck R, Wood WI, Harkins RN, Tuddenham EG, Lawn RM, Capon DJ. Structure of human factor VIII. Nature 1984; 312:337–342.
38. Hoyer LW, Drohan WN, Lubon H. Production of human therapeutic proteins in transgenic animals. Vox Sang 1994;67 Suppl 3:217–220.
39. Fay PJ. Activation of factor VIII and mechanisms of cofactor action. Blood Rev 2004;18:1–15.
40. Pittman DD, Kaufman RJ. Proteolytic requirements for thrombin activation of anti-hemophilic factor (factor VIII). Proc Natl Acad Sci USA 1988;85:2429–2433.
41. Fay PJ, Smudzin TM. Characterization of the interaction between the A2 subunit and A1/A3-C1-C2 dimer in human factor VIIIa. J Biol Chem 1992;267:13246–13250.
42. Wakabayashi H, Fay PJ. Identification of residues contributing to A2 domain-dependent structural stability in factor VIII and factor VIIIa. J Biol Chem 2008;283:11645–11651.
43. Shen BW, Spiegel PC, Chang CH, Huh JW, Lee JS, Kim J, Kim YH, Stoddard BL. The tertiary structure and domain organization of coagulation factor VIII. Blood 2008;111:1240–1247.
44. Derrick TS, Kashi RS, Durrani M, Jhingan A, Middaugh CR. Effect of metal cations on the conformation and inactivation of recombinant human factor VIII. J Pharm Sci 2004;93:2549–2557.
45. Ngo JC, Huang M, Roth DA, Furie BC, Furie B. Crystal structure of human factor VIII: implications for the formation of the factor IXa–factor VIIIa complex. Structure 2008;16:597–606.
46. Fay PJ, Haidaris PJ, Smudzin TM. Human factor VIIIa subunit structure. Reconstruction of factor VIIIa from the isolated A1/

A3-C1-C2 dimer and A2 subunit. J Biol Chem 1991;266:8957–8962.
47. Lollar P, Parker CG. pH-dependent denaturation of thrombin-activated porcine factor VIII. J Biol Chem 1990;265:1688–1692.
48. Pipe SW, Eickhorst AN, McKinley SH, Saenko EL, Kaufman RJ. Mild hemophilia A caused by increased rate of factor VIII A2 subunit dissociation: evidence for nonproteolytic inactivation of factor VIIIa in vivo. Blood 1999;93:176–183.
49. Svensson LA, Thim L, Olsen OH, Nicolaisen EM. Evaluation of the metal binding sites in a recombinant coagulation factor VIII identifies two sites with unique metal binding properties. Biol Chem 2013;394:761–765.
50. Thim L, Vandahl B, Karlsson J, Klausen NK, Pedersen J, Krogh TN, Kjalke M, Petersen JM, Johnsen LB, Bolt G, Norby PL, Steenstrup TD. Purification and characterization of a new recombinant factor VIII (N8). Haemophilia 2010;16:349–359.
51. Doering CB, Healey JF, Parker ET, Barrow RT, Lollar P. High level expression of recombinant porcine coagulation factor VIII. J Biol Chem 2002;277:38345–38349.
52. Ritchie TK, Grinkova YV, Bayburt TH, Denisov IG, Zolnerciks JK, Atkins WM, Sligar SG. Chapter 11—Reconstitution of membrane proteins in phospholipid bilayer nanodiscs. Methods Enzymol 2009; 464:211–231.
53. Mastronarde DN. Automated electron microscope tomography using robust prediction of specimen movements. J Struct Biol 2005; 152:36–51.
54. Kremer JR, Mastronarde DN, McIntosh JR. Computer visualization of three-dimensional image data using IMOD. J Struct Biol 1996; 116:71–76.
55. Tang G, Peng L, Baldwin PR, Mann DS, Jiang W, Rees I, Ludtke SJ. EMAN2: an extensible image processing suite for electron microscopy. J Struct Biol 2007;157:38–46.
56. Wakabayashi H, Varfaj F, Deangelis J, Fay PJ. Generation of enhanced stability factor VIII variants by replacement of charged residues at the A2 domain interface. Blood 2008;112: 2761–2769.
57. Egelman EH. A robust algorithm for the reconstruction of helical filaments using single-particle methods. Ultramicroscopy 2000;85: 225–234.
58. Egelman EH. The iterative helical real space reconstruction method: surmounting the problems posed by real polymers. J Struct Biol 2007;157:83–94.
59. Miller J, Dalm D, Koyfman AY, Grushin K, Stoilova-McPhie S. Helical Organization of Blood Coagulation Factor VIII on Lipid Nanotubes. J Vis Exp 2014;88.
60. Grushin K, Miller J, Dalm D, Parker ET, Healey JF, Lollar P, Stoilova-McPhie S. Lack of recombinant factor VIII B-domain induces phospholipid vesicle aggregation: implications for the immunogenicity of factor VIII. Haemophilia 2014.
61. Gatti L, Mannucci PM. Use of porcine factor VIII in the management of seventeen patients with factor VIII antibodies. Thromb Haemost 1984;51:379–384.
62. Lusher JM. First and second generation recombinant factor VIII concentrates in previously untreated patients: recovery, safety, efficacy, and inhibitor development. Semin Thromb Hemost 2002;28:273–276.
63. Pettersen EF, Goddard TD, Huang CC, Couch GS, Greenblatt DM, Meng EC, Ferrin TE. UCSF Chimera—a visualization system for exploratory research and analysis. J Comput Chem 2004;25:1605–1612.
64. Goddard TD, Ferrin TE. Visualization software for molecular assemblies. Curr Opin Struct Biol 2007;17:587–595.
65. Goddard TD, Huang CC, Ferrin TE. Visualizing density maps with UCSF Chimera. J Struct Biol 2007;157:281–287.
66. Pintilie G, Chiu W. Comparison of Segger and other methods for segmentation and rigid-body docking of molecular components in cryo-EM density maps. Biopolymers 2012;97:742–760.
67. Duffy EJ, Parker ET, Mutucumarana VP, Johnson AE, Lollar P. Binding of factor VIIIa and factor VIII to factor IXa on phospholipid vesicles. J Biol Chem 1992;267:17006–17011.